Red Light Treatment in an Axotomy Model of Neurodegeneration

Kathy Beirne [1,2], Malgorzata Rozanowska [1,2], Marcela Votruba *[1, 2,3]

1. School of Optometry and Vision Sciences Cardiff University, Cardiff, UK

2. Cardiff Institute for Tissue Engineering and Repair, Cardiff University, Cardiff, UK

3. Cardiff Eye Unit, University Hospital of Wales, Cardiff, UK

*Corresponding author email: VotrubaM@cardiff.ac.uk (Marcela Votruba)

ABSTRACT

Red light has been shown to provide neuroprotective effects. Axotomising the optic nerve initiates retinal ganglion cell (RGC) degeneration, and an early marker of this is dendritic pruning. We hypothesised that 670 nm light can delay axotomy induced dendritic pruning in the retinal explant. To test this hypothesis, we monitored the effects of 670 nm light (radiant exposure of 31.7 J/cm^2), on RGC dendritic pruning in retinal explants from C57BL/6J mice, at 40 minutes, 8 hours and 16 hours post axotomy. For sham-treated retinae, area under the Sholl curve, peak of the Sholl curve and dendritic length at 8 hours post axotomy showed statistically significant reductions by 42.3% (p=0.008), 29.8% (p=0.007) and 38.4% (p=0.038), respectively, which were further reduced after 16 hours by 40.56% (p<0.008), 33.9% (p<0.007), 45.43% (p<0.006), respectively. Dendritic field area was also significantly reduced after 16 hours, by 44.23% (p<0.019). Such statistically significant reductions were not seen in light-treated RGCs at 8 or 16 hours post axotomy. The results demonstrate the ability of 670 nm light to partially prevent *ex vivo* dendropathy in the mouse retina, suggesting that it is worth exploring as a treatment option for dendropathy associated neurodegenerative diseases, including glaucoma and Alzheimer's disease.

INTRODUCTION

Evidence is continually mounting in support of the potential of red and near infrared (NIR) light therapy to provide protective effects in various neurodegenerative diseases including Parkinson's disease and multiple sclerosis [1-3]. Red/NIR light therapy has also shown great potential in the treatment of the more acute neurodegenerative conditions such as stroke, spinal cord injury and traumatic brain injury [1, 4-11].

Since longer wavelengths have the ability to penetrate deeper than shorter wavelengths, NIR light is the preferred choice for irradiating brain tissue [12]. When irradiating the retina however the issue of tissue penetration, when using shorter wavelengths, is avoided. Consequently, the beneficial effects of red light have been reported in the retina. Treatment with 670 nm light has provided protection against cell loss in various rodent models of photoreceptor damage whilst demonstrating the safety of using 670 nm light with an irradiance of 60 mW/cm^2 on this light sensitive tissue [13, 14]. Also, 670 nm light provided protection in other models retinal damage or dysfunction [15-18]. In particular, treatment with 670 nm light in a rat model of partial axotomy (optic nerve transection) resulted in improved vision, 7 days post injury [19].

Apoptosis, the primary mechanism of retinal ganglion cell (RGC) death following axotomy, has been shown to be delayed until 3-4 days after axotomy, *in vivo* [20]. RCG dendritic pruning, as characterized by a reduction in dendritic complexity, reduced dendritic arbor area and shrinkage of dendrites, has been observed in mouse models of both glaucoma and Alzheimer's disease and this event has been suggested to precede cell loss [21-23].

Until recently, the mechanisms by which dendrites are eliminated from the neuron were largely unknown. Newly emerging data has provided some mechanistic insight into this process. The findings of one such study has suggested that dendrite degeneration occurs in a process independent of apoptosis involving a local loss of mitochondrial membrane potential and ATP decline, which precede dendrite loss [24]. Inflammation is, likewise, thought to play a prominent role in this process, as an increase in the pro-inflammatory cytokine, interferon γ, and an upregulation in complement proteins were found to be associated with the dendritic pruning that occurs in neurodegenerative diseases and neural injury [25, 26]. Other findings have shown the inhibition of mTOR, the key signal integrator for a variety of extracellular signals including growth factors, to be involved in dendritic pruning [27]. Notably, cellular stressors such as low ATP levels and inflammation have been shown to inhibit mTOR, and optic nerve lesion has been shown to bring about the inhibition of an mTOR complex, an event which has been shown to coincide with dendritic retraction.

Red/NIR light, which is absorbed by complex IV of the mitochondrial electron transport chain, has been shown to upregulate the enzymatic activity of complex IV, increase the mitochondrial membrane potential and increase ATP production [28-34]. Red light was also found to have an anti-inflammatory effect as markers of inflammation, including complement proteins, were significantly reduced in the outer retina following 670 nm light treatment [30, 31, 35-37]. Additionally, red/NIR light was found to modify cell growth by modulating the Akt/mTOR signaling pathway in cancer cells [38]. In fact, the PI3K/Akt/mTOR pathway, which is involved with cell growth, proliferation, differentiation and survival, has been reported to be one of the most studied pathways that is influenced by red/NIR light [39].

Clearly, many of the mechanisms proposed to be involved in the dendritic pruning process are potential therapeutic targets of the molecular mechanism responsible for the beneficial effects of 670 nm light. Therefore, we have hypothesised that 670 nm light can delay the dendritic pruning that is initiated upon axotomy. To test this hypothesis we used an *ex vivo* model of dendritic pruning in the mouse retinal explant. Explanting the retina which involves axotomy of the entire population of RGCs by complete severing of their axons, is rapidly followed by pruning of the RGC dendrites [27]. The retinal explant, consequently, provides a platform upon which to test the effects of 670 nm light on dendritic pruning in a substantially shorter timeframe than would be possible in the aforementioned models of RGC degeneration. The effect of 670 nm light on the RGC dendritic pruning in the retinal explant was monitored at 40 minutes, 8 hours and 16 hours post axotomy. Changes in RGC dendritic morphology over time were investigated by employing various methods to analyze dendritic complexity, including Sholl analysis, area under the Sholl curve, the maximum peak of the Sholl curve, average total dendritic length and average dendritic field area.

MATERIALS AND METHODS

Animals used: Twenty five wild-type, 9 week old, male C57 BL/6J mice were used as the source of retinal explants. Each mouse contributed a maximum of one retina per experimental condition.

Mice were kept in a 12 hour light (4.88 lux of warm white fluorescent lighting with an irradiance of 0.7 $\mu W/cm^2$) / 12 hour light-dark cycle with food and water available *ad libitum.* Maintenance and all experimental procedures were in compliance with the *ARVO Statement*

for the Use of Animals in Ophthalmic and Vision Research and were approved by the Home Office, UK.

Red light treatment: Mice were killed by cervical dislocation under 275 lux of warm white fluorescent light (providing total irradiance of 74 μW/ cm^2 and an irradiance of 2.8 μW/cm^2 in the 600-780 nm range of the electromagnetic spectrum). Retinae were then dissected under 676 lux of warm white fluorescent light (providing a total irradiance of 250 μW/ cm^2 and an irradiance of 130 μW/cm^2 in the red range). Retinae were dissected as described previously and flat mounted onto a 0.4 μm pore PTFE membrane culture plate insert [40]. One retina per mouse was assigned to sham treatment and the other to light treatment. The insert was placed in a 6-well plate containing pre-warmed Neurobasal A media (Invitrogen) at 37 °C.

Red light was delivered to the retinae from a WARP 10 light source (Quantum devices, Inc., Wisconsin, USA), immediately after flat mounting. Red light-treated retinae were exposed to 670 ±15 nm (half width half maximum, HWHM) light with a fluence of 31.7 J/cm², delivered by 6 sequential 88 second exposures of the WARP 10 light device, over a 10 minute period, at room temperature (see Supplementary Materials). Sham treated retinae were placed, at room temperature, in a separate room to the light treatment. Upon cessation of the treatment, the retinae were labelled using DiOlistics, either immediately or after an *ex vivo* period of 8 or 16 hours in a dark incubator, at 37 °C.

DiOlistic labelling of retinal ganglion cells: Retinal ganglion cells were labelled with lipophilic fluorescent dyes to facilitate imaging of the RGC soma, dendrites and axon. 1,10-dioleyl-3,3,3,3 tetramethylindocarbocyanine methanesulphonate (DiO) (Invitrogen) or 3,3'dihexadecyloxacarbocyanine perchlorate (DiI) coated tungsten particles were prepared

prior to retinal preparation, as described previously [40], which was modified from the original protocol [41]. DiOlistic labelling of retinal ganglion cells and the preparation of retinae for imaging was described previously [40]. Retinae were shot once at 100 psi using a Helios gene gun (Bio-Rad) 3 cm from the retina through a 3 µm pore size, high pore density cell culture insert (Milipore), to deliver the dye coated particles to the RGCs. After DiOlistic labelling the explants were transferred to a 5% CO_2 incubator at 37 °C for 30 minutes, to facilitate diffusion of the dye throughout the cells. The retinae were fixed with 4% paraformaldehyde before staining with TO-PRO nuclear stain. The retinae examined in the initial, second and third time points were fixed 40 minutes, 8 hours and 16 hours, respectively, post axotomy.

Analysis of RGC dendritic complexity: RGC images were acquired with a Zeiss LSM 510 confocal microscope (Carl Zeiss, Ltd, UK), using a 20X (0.8 NA) objective lens, 543 nm excitation and BP 565-615 nm emission filter for DiI, 488 nm excitation and BP 500-530 nm emission filter for DiO and 633 excitation and 651-704 nm emission spectral window for TO-PRO.

Images stacks were collected each 1 µm distance along the Z-plane, from the ganglion cell layer to the inner nuclear layer, producing a reconstructed 3-dimensional image. The experimental groups to which the cells belonged to were masked using a Fiji plugin prior to tracing [42]. Dendrites were traced using the Fiji plugin Simple Neurite Tracer [43], to facilitate Sholl analysis using the automated Sholl analysis Fiji plugin. Sholl analysis [44] quantitatively measures dendritic complexity, counting the number of dendritic intersections with concentric rings placed at 10 µm intervals from the soma centre to the most peripheral dendrite.

To facilitate statistical comparison, obtaining the area under the Sholl curve for individual RGCs was required. The area under the Sholl curve was obtained by integration of the area under a 5 parameter Weibull curve fitted to the Sholl data of individual cells in Sigma Plot using the following equation:

$$y = y_0 + a\left(\frac{c-1}{c}\right)^{\frac{1-c}{c}} * \left[\frac{x-x_0}{b} + \left(\frac{c-1}{c}\right)^{\frac{1}{c}}\right]^{c-1} * e^{-\left[\frac{x-x_0}{b} + \left(\frac{c-1}{c}\right)^{\frac{1}{c}}\right]^{c}} + \left(\frac{c-1}{c}\right)$$

Where a, b, c, x_0, y_0 are the fitted parameters, y is the number of intersections of dendrites with concentric rings placed at 10 µm intervals from the soma centre to the most peripheral dendrite and x is the distance from the RGC soma centre.

The total dendritic length was calculated from the sum of lengths of each dendritic path measured in Simple Neurite Tracer plugin of Fiji. The dendritic field area of the RGC was obtained by connecting the ends of each dendrite using a polygon tool in Fiji.

Statistical analyses: The Shapiro-Wilk test was performed in SPSS to test for normality in the data. Non-parametric data were analysed using a Mann-Whitney *U* test in SPSS. *p* values less of than 0.05 were considered statistically significant.

RESULTS

A total of 31 retinae out of 50 included RGCs with fluorescent labeling that allowed for accurate tracing of their dendrites followed by Sholl analysis (Figure 1).

Sholl analysis is a method used to analyze dendritic morphology, which gives information on the functionality of the neuron and its ability communicate effectively with other cells [45].

Since dendrites are the main regions of information input into neurons, reductions in the number of dendrites could hinder the ability of the RCG to receive information from the preceding bipolar and amacrine cells. Changes in dendritic morphology are associated with malfunction in neurons, as seen in neurodegenerative diseases. Sholl analysis enables the monitoring of these changes quantitatively by producing the data in the form of a Sholl profile.

In this experiment, the Sholl profile, which illustrates the number of intersections of dendrites with concentric rings placed at each 10 μm distance from the cell soma, of RGCs from sham treated retinae showed a downward and leftward shift after both 8 and 16 hours *ex vivo*, indicating a loss of RGC dendritic complexity over time (Figure 1C). In retinae treated with red light, the leftward shift in the RGC Sholl profile over time was less profound (Figure 1D). There was a statistically significant reduction in the number of dendritic intersections at 70, 90 and 130 μm from the soma after 8 hours ($p<0.05$) and at 30 ($p<0.05$), 40 ($p<0.01$), 50 ($p<0.05$), 60-70 ($p<0.01$) and 80-110 μm ($p<0.05$) after 16 hours *ex vivo* for sham-treated retinae. In contrast, RGCs from light treated retinae had no statistically significant reductions in the number of dendritic intersections at any point on the Sholl curve after 8 or 16 hours.

<Figure 1>

The Sholl profile suggests that there is a difference in the area under the Sholl curve and the maximum number of dendritic intersections in the Sholl plot. For statistical comparison however, it was necessary to compare the Sholl profiles of the individual RGCs used to create the Sholl plots in Figure 1. This was achieved by fitting a curve to the Sholl plot of each cell and doing subsequent analysis using the entire population of neurons, allowing statistical comparisons to be made.

A 5 parameter Weibull curve, fitted to each RGC, enabled the calculation of the average area under the fitted curves and the average peak of the fitted curves for each experimental group (Figure 2A). The average area under the fitted Sholl curves, of RGCs from sham treated retinae was reduced from 2042 a.u. at 40 minutes to 1177 a.u. after 8 hours *ex vivo* (p=0.008) and to 1213 a.u. after 16 hours (p=0.016) (Figure 2B). For light-treated retinae the values were reduced from 2186 a.u. after 40 minutes to 1804 a.u. after 8 hours and to 1706 a.u. after 16 hours but none of the differences were significant (p=0.561 and p=0.232, respectively) (Figure 2B).

The average maximum peak of the fitted curves for RGCs from sham-treated retinae was significantly reduced from 22.1 intersections at 40 minutes to 15.5 intersections at 8 hours (p=0.007) and to 14.6 intersections at 16 hours (p=0.007). In RGCs from light-treated retinae, the average maximum peak of the fitted curves was reduced from 22.1 at 40 minutes to only 20.0 intersections after 8 hours and to 17.3 a.u after 16 hours (p=0.639 and p=0.113, respectively) (Figure 2C).

<Figure 2>

The fitted curves then underwent additional analyses to explore the initial rate of branching of the Sholl curve from the soma to the half maximum of the Sholl peak (Figure 3A). The initial rate of branching provides information on the extent of proximal branching of the RGC dendritic arbor. The rate of decay of the Sholl curve was also measured to explore the extent of branching from the peak of the Sholl curve to the half maximum (Figure 3B). This parameter yields information on the extent of branching occurring in the more distal region of the RGC's dendritic arbor.

199 In RGCs from sham-treated retinae, there was no statistically significant change in the rate of
200 growth of the Sholl curve from the soma to the half maximum of the Sholl peak from 40
201 minutes to 8 hours (0.49 to 0.38, p=0.125) or from 40 minutes to 16 hours (0.49 to 0.52,
202 p=0.910) indicating that the branching of the most proximal dendrites was not altered up to 16
203 hours post axotomy. Similarly, changes in the rate of decay of the Sholl curve from the
204 maximum to the half maximum, in sham-treated retinae, were found not to be statistically
205 significantly different: 0.27 at 40 minutes, 0.22 after 8 hours (p=0.170 when compared to the
206 value at 40 minutes) and 0.20 after 16 hours (p=0.052 when compared to the value at 40
207 minutes) in sham-treated RGCs.
208 <Figure 3>
209 To further investigate the effects of red light on RGC dendrites after axotomy, measurements
210 of dendritic field area and total dendritic length, which are additional measures of RGC
211 dendritic complexity were obtained. Dendritic field area provides information on how widely
212 the cell spreads over the retina and relates to the size of its receptive field. Since RGCs are the
213 final neurons in the visual pathway before the light signal is transmitted to the brain, a
214 reduction in the area of the RGC dendritic field could diminish photosensitivity, impeding the
215 entire visual process. Similarly, since total dendritic length has been found to be positively
216 correlated with whole-neuron capacitance [46], a decrease in this parameter could negatively
217 impact on the ability of the cell to reach the threshold for electrical stimulation, thereby
218 reducing the likelihood of an action potential being formed.
219 The average dendritic field area for RGCs from sham-treated retinae decreased significantly
220 from 31204 μm^2 at 40 minutes to 17402 μm^2 after 16 hours *ex vivo* (p=0.019). Contrastingly,
221 where retinae were treated with 670 nm light, the RGCs did not experience a statistically

222 significant reduction in their average dendritic field area (28971 to 22540 μm^2, p=0.195)
223 (Figure 4B).
224 A statistically significant decrease in the average total dendritic length was also seen in RGCs
225 from sham treated retinae, from 3007 μm at 40 minutes to 1851 μm at 8 hours (p=0.038) and
226 to 1640 μm at 16 hours (p=0.006). The values for dendritic length decreased from 2943 μm to
227 2430 μm after 8 hours (p=0.286) and 2362 after 16 hours (p=0.170), in RGCs that were
228 exposed to 670 nm light, but the differences were not statistically significant (Figure 5B).
229 Although the average total dendritic field area of red light-treated retinae was 30% greater than
230 in the sham-treated retinae after 16 hours, the difference was not statistically significant
231 (p=0.385).To determine the number of retinae required to obtain a statistically significant
232 difference between red light and sham-treated retinae after 16 hours, a sample size calculation
233 was done. It was determined that 40 additional retinae would be required for the sham-treated
234 group and 61 for the red light-treated group to achieve a statistically significant difference in
235 the dendritic field area between sham and red light-treated retinae after 16 hours at 0.8 power.
236 <Figure 4>
237 <Figure 5>
238 In summary, the statistically significant reductions in the number of RGC dendritic
239 intersections at various points on the Sholl plot were observed after 8 and 16 hours in sham-
240 treated retinae but were not seen in red light-treated retinae. Treatment with red light also
241 prevented a statistically significant reduction to the area under the Sholl curve and to the peak
242 of the Sholl curve. The results for average dendritic field area and average total dendritic
243 length measurements were consistent with Sholl analysis data, showing the ability of 670 nm
244 light to prevent statistically significant decreases in further parameters of dendritic complexity.

Red light prevented statistically significant reductions in the total loss of dendrites form the entire RGC dendritic arbor, the total area of the dendritic field and the loss of dendrites from the most densely branched region of the RGC dendritic arbor.

DISCUSSION

Herein we report, for the first time, of the ability of 670 nm light to prevent the dendritic pruning that occurs upon axonal injury. In this study, we investigated the effect of 670 nm light on RGC dendritic pruning which occurs in the mouse retinal explant upon axotomy of the optic nerve. This degeneration was detectable by analysis of dendritic morphology after 8 hours and again after 16 hours, where statistically significant decreases from initial values were observed in sham-treated explants. Sholl analysis revealed statistically significant reductions in the number of dendritic intersections at various points of the Sholl curve after both 8 and 16 hours. The area under the Sholl curve, the average peak of the fitted Sholl curve, the average total dendritic length and average dendritic field area after 16 hours also showed statistically significant reductions from the values at 40 minutes by 40.56% (p<0.008), 33.9% (p<0.007), 45.43% (p<0.006), and 44.23% (p<0.019), respectively. Our results have demonstrated that 670 nm light can prevent the statistically significant reductions in these measurements up to 16 hours post axotomy, since the reductions seen in RGCs from light treated retinae were smaller and not statistically significant. The results revealed that rapid intervention with 670 nm light, when administered immediately after the acute optic nerve lesion, axotomy, prevented significant neuronal damage.

Evidence has been gathered, suggestive of a role for dendritic abnormalities in the pathology associated with the initial clinical symptoms of a range of neurodegenerative diseases [27]. Degeneration of RGCs is a hallmark of devastating retinal degenerative diseases such as glaucoma and autosomal dominant optic atrophy (ADOA). A progressive degeneration of the RGCs in such diseases coincides with deterioration in visual acuity, eventually resulting in blindness. In experimental glaucoma, dendritic pruning has been suggested to precede selective loss of RGCs [47-49]. Also in ADOA, dendritic pruning was found to begin at a time when a loss in visual acuity was observed, in a mouse model of the disease [40].

The effect of changes to the dendritic morphology of neurons has also been observed in some of the most common and debilitating, neurodegenerative diseases, including Alzheimer's disease. In the postmortem brains of Alzheimer's disease patients, there was a marked decrease in the number of dendritic branches in the majority of neurons from the visual and acoustic cortices compared to normal controls [50]. In addition, there was a 45% decrease in the dendritic field area compared with controls in these neurons. Alterations in dendritic morphology has also been found in Parkinson's disease [51]. In the *substantia nigra pars compacta* of *post mortem* tissue from Parkinson's disease patients, there was a severe reduction in the dendritic length of dopaminergic type I neurons compared with healthy controls [52]. Similarly, in post mortem tissue from patients with multiple sclerosis (MS), a loss in dendritic arborization was observed in cortical lesions [53]. This pathology was thought to contribute to the clinical symptoms of MS by decreasing the synaptic input to the cortex. Since these relatively subtle changes to the neurons are thought play a role in the clinical symptoms, mild beneficial effect on the survival ability of the dendrites could translate into a

significant clinical effect. Delaying the dendritic pruning that occurs in the early stages of these neurodegenerative diseases could delay the onset of clinical symptoms, thereby providing an invaluable improvement to the quality of life of patients.

The pathology for the initial symptoms in the discussed diseases appears to be due to a loss of dendrites as opposed to cell death. Moreover, dendritic degeneration appears to occur via a process independent of neuronal loss. It was found that the inhibition of pro-apoptotic proteins was sufficient to delay neuronal somal death while failing to have any preventative effect on dendritic pruning [54]. Therefore, looking at ways of preventing dendritic pruning may require a unique approach and may also be a more fruitful treatment strategy than merely endeavoring to keep dysfunctional cells alive.

Our understanding of the pathology of neurodegenerative diseases seems to be changing from one of progressive cell loss to one whereby more subtle alterations in the dendritic morphology are associated with the initial clinical symptoms. The alterations to the dendritic morphology reported in the aforesaid neurodegenerative diseases were similar to those changes observed in the current experiment after 16 hours post axotomy, in the retinal explant. Since rapid intervention with 670 nm light treatment prevented such statistically significant alterations in the dendritic morphology for up to 16 hours *ex vivo*, it is possible that it may prevent or slow down the changes to the dendrites associated with the pathology of the said neurodegenerative diseases.

ACKNOWLEDGMENTS

This study was supported by Fight for Sight, UK. We thank Nick White for help with confocal microscopy and 3D image analysis. We also thank Dr. Pratyusha Ganne for her assistance with retinal dissections.

SUPPLEMENTARY MATERIALS

Figure S1 can be found at DOI: 10.1562/2006-xxxxxx.s1.

REFERENCES

1. Naeser, M.A. and M.R. Hamblin (2011) Potential for transcranial laser or LED therapy to treat stroke, traumatic brain injury, and neurodegenerative disease. Photomedicine and laser surgery. 29(7), 443-446.

2. Oueslati, A., B. Lovisa, J. Perrin, G. Wagnières, H. Van Den Bergh, Y. Tardy, and H.A. Lashuel (2015) Photobiomodulation suppresses alpha-synuclein-induced toxicity in an aav-based rat genetic model of Parkinson's disease. PloS one. 10(10), e0140880.

3. Muili, K.A., S. Gopalakrishnan, J.T. Eells, and J.-A. Lyons (2013) Photobiomodulation induced by 670 nm light ameliorates mog35-55 induced EAE in female C57BL/6 mice: A role for remediation of nitrosative stress. PloS one. 8(6), e67358.

4. Fitzgerald, M., S. Hodgetts, C. Van Den Heuvel, R. Natoli, N.S. Hart, K. Valter, A.R. Harvey, R. Vink, J. Provis, and S.A. Dunlop (2013) Red/near-infrared irradiation therapy for treatment of central nervous system injuries and disorders. Reviews in the Neurosciences. 24(2), 205-226.

5. Byrnes, K.R., R.W. Waynant, I.K. Ilev, X. Wu, L. Barna, K. Smith, R. Heckert, H. Gerst, and J.J. Anders (2005) Light promotes regeneration and functional recovery and alters the immune response after spinal cord injury. Lasers in surgery and medicine. 36(3), 171-185.

6. Wu, Q., W. Xuan, T. Ando, T. Xu, L. Huang, Y.Y. Huang, T. Dai, S. Dhital, S.K. Sharma, and M.J. Whalen (2012) Low-level laser therapy for closed-head traumatic brain injury in mice: Effect of different wavelengths. Lasers in surgery and medicine. 44(3), 218-226.

7. Xuan, W., T. Agrawal, L. Huang, G.K. Gupta, and M.R. Hamblin (2015) Low-level laser therapy for traumatic brain injury in mice increases brain derived neurotrophic factor (BDNF) and synaptogenesis. Journal of biophotonics. 8(6), 502-511.

8. Naeser, M.A. and M.R. Hamblin (2015) Traumatic brain injury: A major medical problem that could be treated using transcranial, red/near-infrared led photobiomodulation. Photomedicine and laser surgery. 33(9), 443-446.

9. Dong, T., Q. Zhang, M.R. Hamblin, and M.X. Wu. Low level light in combination with metabolic modulators for effective therapy. in SPIE BiOS. 2015. International Society for Optics and Photonics.

10. Ando, T., Y-Y. Huang, and M.R. Hamblin, LLLT for stroke and brain disease. In: Hamblin MR, Huang Y-Y (eds), Handbook of photomedicine. 2013, Boca Raton: CRC Press.

11. Parizotto, N.A., Y-Y. Huang, and M.R. Hamblin, LLLT for nerve and spinal cord regeneration. In: Hamblin MR, Huang Y-Y (eds), Handbook of photomedicine. 2013, Boca Raton: CRC Press.

12. Jagdeo, J.R., L.E. Adams, N.I. Brody, and D.M. Siegel (2012) Transcranial red and near infrared light transmission in a cadaveric model. PloS one. 7(10), e47460.

13. Albarracin, R., R. Natoli, M. Rutar, K. Valter, and J. Provis (2013) 670 nm light mitigates oxygen-induced degeneration in C57BL/6J mouse retina. BMC neuroscience. 14(1), 1.

14. Albarracin, R., J. Eells, and K. Valter (2011) Photobiomodulation protects the retina from light-induced photoreceptor degeneration. Investigative ophthalmology & visual science. 52(6), 3582-3592.

15. Peoples, C., V.E. Shaw, J. Stone, G. Jeffery, G.E. Baker, and J. Mitrofanis (2012) Survival of dopaminergic amacrine cells after near-infrared light treatment in MPTP-treated mice. ISRN neurology. 2012.

16. Tang, J., Y. Du, C.A. Lee, R. Talahalli, J.T. Eells, and T.S. Kern (2013) Low-intensity far-red light inhibits early lesions that contribute to diabetic retinopathy: In vivo and in vitro far-red light inhibits DR. Investigative ophthalmology & visual science. 54(5), 3681-3690.

17. Barbosa, M., R. Natoli, K. Valter, J. Provis, and T. Maddess (2014) Integral-geometry characterization of photobiomodulation effects on retinal vessel morphology. Biomedical optics express. 5(7), 2317-2332.

18. Natoli, R., K. Valter, M. Barbosa, J. Dahlstrom, M. Rutar, A. Kent, and J. Provis (2013) 670nm photobiomodulation as a novel protection against retinopathy of prematurity: Evidence from oxygen induced retinopathy models. PloS one. 8(8), e72135.

19. Giacci, M.K., L. Wheeler, S. Lovett, E. Dishington, B. Majda, C.A. Bartlett, E. Thornton, E. Harford-Wright, A. Leonard, and R. Vink (2014) Differential effects of 670 and 830 nm red near infrared irradiation therapy: A comparative study of optic nerve injury, retinal degeneration, traumatic brain and spinal cord injury.

20. Magharious, M.M., P.M. D'Onofrio, and P.D. Koeberle (2011) Optic nerve transection: A model of adult neuron apoptosis in the central nervous system. Journal of visualized experiments: JoVE, (51).

21. Berry, R.H., J. Qu, S.W. John, G.R. Howell, and T.C. Jakobs (2015) Synapse loss and dendrite remodeling in a mouse model of glaucoma. PloS one. 10(12), e0144341.

22. Votruba, M., P.A. Williams, R.A. Thirgood, H. Oliphant, M.A. Good, J. Williams, and J.E. Morgan (2012) Retinal ganglion cell dendritic degeneration in a mouse model of alzheimer's disease. Investigative Ophthalmology & Visual Science. 53(14), 4650-4650.

23. Williams, P.A., R.A. Thirgood, H. Oliphant, A. Frizzati, E. Littlewood, M. Votruba, M.A. Good, J. Williams, and J.E. Morgan (2013) Retinal ganglion cell dendritic degeneration in a mouse model of Alzheimer's disease. Neurobiology of aging. 34(7), 1799-1806.

24. Ikegami, K. and T. Koike (2003) Non-apoptotic neurite degeneration in apoptotic neuronal death: Pivotal role of mitochondrial function in neurites. Neuroscience. 122(3), 617-626.

25. Kim, I.-J., H.N. Beck, P.J. Lein, and D. Higgins (2002) Interferon γ induces retrograde dendritic retraction and inhibits synapse formation. The Journal of neuroscience. 22(11), 4530-4539.

26. Stephan, A.H., B.A. Barres, and B. Stevens (2012) The complement system: An unexpected role in synaptic pruning during development and disease. Annual review of neuroscience. 35, 369-389.

27. Di Polo, A. (2015) Dendrite pathology and neurodegeneration: Focus on mTOR. Neural regeneration research. 10(4), 559.

391 28. Karu, T. (2008) Action spectra: Their importance for low level light therapy.
392 Photobiological Sciences Online (KC Smith, editor) American Society for Photobiology,
393 http://www. photobiology. info.
394 29. Hamblin, M.R. and T.N. Demidova. Mechanisms of low level light therapy. in Biomedical
395 Optics 2006. 2006. International Society for Optics and Photonics.
396 30. Kokkinopoulos, I., A. Colman, C. Hogg, J. Heckenlively, and G. Jeffery (2013) Age-
397 related retinal inflammation is reduced by 670 nm light via increased mitochondrial membrane
398 potential. Neurobiology of aging. 34(2), 602-609.
399 31. Begum, R., M.B. Powner, N. Hudson, C. Hogg, and G. Jeffery (2013) Treatment with 670
400 nm light up regulates cytochrome c oxidase expression and reduces inflammation in an age-
401 related macular degeneration model. PloS one. 8(2), e57828.
402 32. Ferraresi, C., M.V.P. de Sousa, Y.-Y. Huang, V.S. Bagnato, N.A. Parizotto, and M.R.
403 Hamblin (2015) Time response of increases in atp and muscle resistance to fatigue after low-
404 level laser (light) therapy (LLLT) in mice. Lasers in medical science. 30(4), 1259-1267.
405 33. Ferraresi, C., N.A. Parizotto, M.V. Pires de Sousa, B. Kaippert, Y.Y. Huang, T. Koiso,
406 V.S. Bagnato, and M.R. Hamblin (2015) Light-emitting diode therapy in exercise-trained mice
407 increases muscle performance, cytochrome c oxidase activity, atp and cell proliferation.
408 Journal of biophotonics. 8(9), 740-754.
409 34. Karu, T., Y-Y. Huang and M.R. Hamblin, Chromophores (photoacceptors) for LLLT. In:
410 Hamblin MR, Huang Y-Y (eds), Handbook of photomedicine. 2013, Boca Raton: CRC Press.
411 35. Fernandes, K.P.S., N.H.C. Souza, R.A. Mesquita-Ferrari, D.d.F.T. da Silva, L.A. Rocha,
412 A.N. Alves, K. de Brito Sousa, S.K. Bussadori, M.R. Hamblin, and F.D. Nunes (2015)
413 Photobiomodulation with 660-nm and 780-nm laser on activated j774 macrophage-like cells:

414 Effect on M1 inflammatory markers. Journal of Photochemistry and Photobiology B: Biology.
415 153, 344-351.
416 36. Rutar, M., R. Natoli, R. Albarracin, K. Valter, and J. Provis (2012) 670-nm light treatment
417 reduces complement propagation following retinal degeneration. J Neuroinflammation. 9, 257.
418 37. Calaza, K.C., J.H. Kam, C. Hogg, and G. Jeffery (2015) Mitochondrial decline precedes
419 phenotype development in the complement factor H mouse model of retinal degeneration but
420 can be corrected by near infrared light. Neurobiology of aging. 36(10), 2869-2876.
421 38. Sperandio, F.F., F.S. Giudice, L. Corrêa, D.S. Pinto, M.R. Hamblin, and S.C. de Sousa
422 (2013) Low-level laser therapy can produce increased aggressiveness of dysplastic and oral
423 cancer cell lines by modulation of AKT/mTOR signaling pathway. Journal of biophotonics.
424 6(10), 839-847.
425 39. Sonis, S.T., S. Hashemi, J.B. Epstein, R.G. Nair, and J.E. Raber-Durlacher (2016) Could
426 the biological robustness of low level laser therapy (photobiomodulation) impact its use in the
427 management of mucositis in head and neck cancer patients. Oral Oncology. 54, 7-14.
428 40. Williams, P.A., J.E. Morgan, and M. Votruba (2010) Opa1 deficiency in a mouse model of
429 dominant optic atrophy leads to retinal ganglion cell dendropathy. Brain, awq218.
430 41. Gan, W.-B., J. Grutzendler, W.T. Wong, R.O. Wong, and J.W. Lichtman (2000)
431 Multicolor “Diolistic” labeling of the nervous system using lipophilic dye combinations.
432 Neuron. 27(2), 219-225.
433 42. Schindelin, J., I. Arganda-Carreras, E. Frise, V. Kaynig, M. Longair, T. Pietzsch, S.
434 Preibisch, C. Rueden, S. Saalfeld, and B. Schmid (2012) Fiji: An open-source platform for
435 biological-image analysis. Nature methods. 9(7), 676-682.

436 43. Longair, M.H., D.A. Baker, and J.D. Armstrong (2011) Simple neurite tracer: Open source
437 software for reconstruction, visualization and analysis of neuronal processes. Bioinformatics.
438 27(17), 2453-2454.
439 44. Sholl, D. (1953) Dendritic organization in the neurons of the visual and motor cortices of
440 the cat. Journal of anatomy. 87(Pt 4), 387.
441 45. Langhammer, C.G., M.L. Previtera, E.S. Sweet, S.S. Sran, M. Chen, and B.L. Firestein
442 (2010) Automated sholl analysis of digitized neuronal morphology at multiple scales: Whole
443 cell sholl analysis versus sholl analysis of arbor subregions. Cytometry Part A. 77(12), 1160-
444 1168.
445 46. Gertler, T.S., C.S. Chan, and D.J. Surmeier (2008) Dichotomous anatomical properties of
446 adult striatal medium spiny neurons. The Journal of neuroscience. 28(43), 10814-10824.
447 47. Liu, M., L. Guo, T. Salt, and M. Cordeiro (2010) Dendritic changes in the retinal ganglion
448 cells in a rat model of experimental glaucoma. Investigative Ophthalmology & Visual Science.
449 51(13), 5217-5217.
450 48. Williams, P.A., G.R. Howell, J.M. Barbay, C.E. Braine, G.L. Sousa, S.W. John, and J.E.
451 Morgan (2013) Retinal ganglion cell dendritic atrophy in DBA/2J glaucoma. PloS one. 8(8),
452 e72282.
453 49. Pavlidis, M., T. Stupp, R. Naskar, C. Cengiz, and S. Thanos (2003) Retinal ganglion cells
454 resistant to advanced glaucoma: A postmortem study of human retinas with the carbocyanine
455 dye dii. Investigative ophthalmology & visual science. 44(12), 5196-5205.
456 50. Baloyannis, S. (2009) Dendritic pathology in Alzheimer's disease. Journal of the
457 neurological sciences. 283(1), 153-157.

458 51. Bertram, L. and R.E. Tanzi (2005) The genetic epidemiology of neurodegenerative disease.
459 The Journal of clinical investigation. 115(6), 1449-1457.
460 52. Patt, S., H.-J. Gertz, L. Gerhard, and J. Cervos-Navarro (1991) Pathological changes in
461 dendrites of substantia nigra neurons in Parkinson's disease: A golgi study.
462 53. Peterson, J.W., L. Bö, S. Mörk, A. Chang, and B.D. Trapp (2001) Transected neurites,
463 apoptotic neurons, and reduced inflammation in cortical multiple sclerosis lesions. Annals of
464 neurology. 50(3), 389-400.
465 54. Koike, T., Y. Yang, K. Suzuki, and X. Zheng (2008) Axon & dendrite degeneration: Its
466 mechanisms and protective experimental paradigms. Neurochemistry international. 52(4), 751-
467 760.

468 **FIGURE CAPTIONS**

469 **Figure 1:** The effect of time *ex vivo* (indicated in the graph legends) on the Sholl profiles of
470 sham (C) and light (D)-treated RGCs. Stars and daggers indicate statistically significant
471 reduction in the number of dendritic intersections, from 40 minutes to 8 hours and 16 hours,
472 respectively. To facilitate comparisons, Sholl profiles of RGCs from sham- and light-treated
473 retinas are shown at 40 minutes (A) and 16 hours (B) ex vivo. * $p<0.05$, ** $p<0.01$, † $p<0.05$,
474 †† $p<0.01$; Mann-Whitney *U* test. Error bars represent SEM.

475 **Figure 2:** The effect of time *ex vivo*, up to 16 hours, on the average area under the fitted
476 curves (B) and average maximum Sholl peaks (C) of sham and light treated RGCs. Stars
477 placed below means indicate statistically significant reductions from the value at 40 minutes,
478 in RGCs from sham-treated retinae. *p* values placed above the means correspond to statistical

comparisons made between light-treated RGCs. *p* values placed next to the means correspond to statistical comparisons made between sham and light-treated RGCs at each time point. (A) A Weibull, 5 parameter curve was fitted to the Sholl data of each individual RGC. Inset: the equation used to create the curve. * $p<0.05$, ** $p<0.01$; Mann-Whitney *U* test. Error bars represent SEM.

Figure 3: The effect of time *ex vivo*, up to 16 hours, on the initial rate of branching of RGC dendrites (A) and the rate of decay of the Sholl curve (B). *p* values placed below the means relate to statistical comparisons made between sham-treated RGCs. *p* values placed above the means correspond to statistical comparisons made between light-treated RGCs. *p* values placed next to the means correspond to statistical comparisons made between sham and light-treated RGCs at each time point. Mann-Whitney *U* test. Error bars represent SEM.

Figure 4: The effect of time *ex vivo*, up to 16 hours, on the average dendritic field area of light and sham treated RGCs. (A) The Z-projected image of an RGC showing the dendritic field area measurement using a polygon tool in ImageJ. Stars placed below the means indicate statistically significant reductions from the value at 40 minutes, in RGCs from sham-treated retinae. Stars and *p* values placed above the means correspond to statistical comparisons made between light-treated RGCs. *p* values placed next to the means correspond to statistical comparisons made between sham and light-treated RGCs at each time point.. * $p<0.01$; Mann-Whitney *U* test. Error bars represent SEM. Arrow indicates the axon. Scale bar represents 100 μm.

Figure 5: The effect of time *ex vivo*, up to 16 hours, on the average dendritic field length of RGCs from sham and light treated retinae. (A) A 3-D image of an RGC tracing used to calculate dendritic field length measurements. (B) Stars placed below the means indicate statistically significant reductions from the value at 40 minutes, in RGCs from sham-treated retinae. *p* values placed above the means correspond to statistical comparisons made between light-treated RGCs. *p* values placed next to the means correspond to statistical comparisons made between sham and light-treated RGCs at each time point. * $p<0.01$, ** $p<0.01$; Mann-Whitney *U* test. Error bars represent SEM. Arrow indicates the axon.

Figure 1

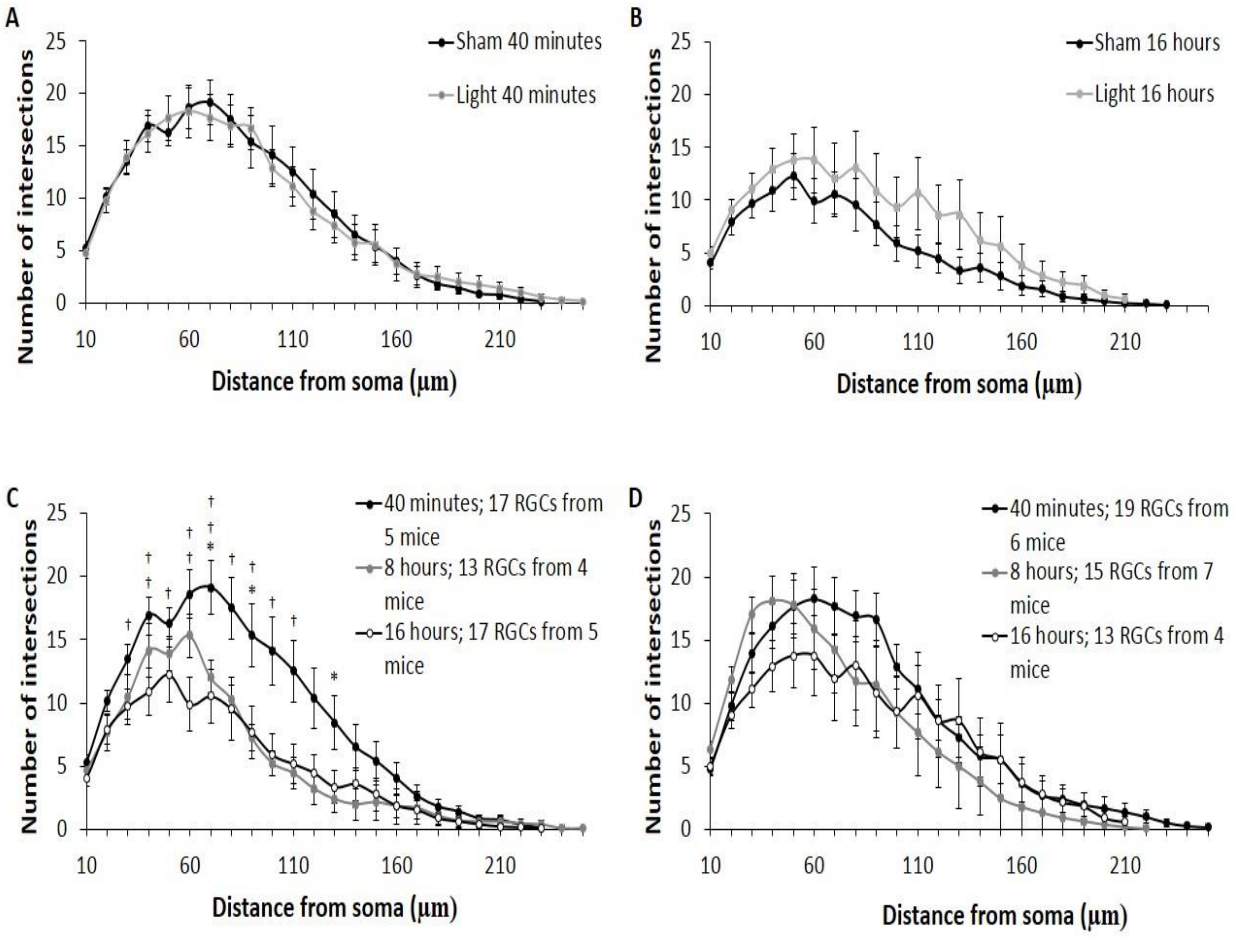
A
Sham 40 minutes
Light 40 minutes
Number of intersections
Distance from soma (µm)
B
Sham 16 hours
Light 16 hours
Number of intersections
Distance from soma (µm)
C
40 minutes; 17 RGCs from 5 mice
8 hours; 13 RGCs from 4 mice
16 hours; 17 RGCs from 5 mice
Number of intersections
Distance from soma (µm)
D
40 minutes; 19 RGCs from 6 mice
8 hours; 15 RGCs from 7 mice
16 hours; 13 RGCs from 4 mice
Number of intersections
Distance from soma (µm)

Figure 2

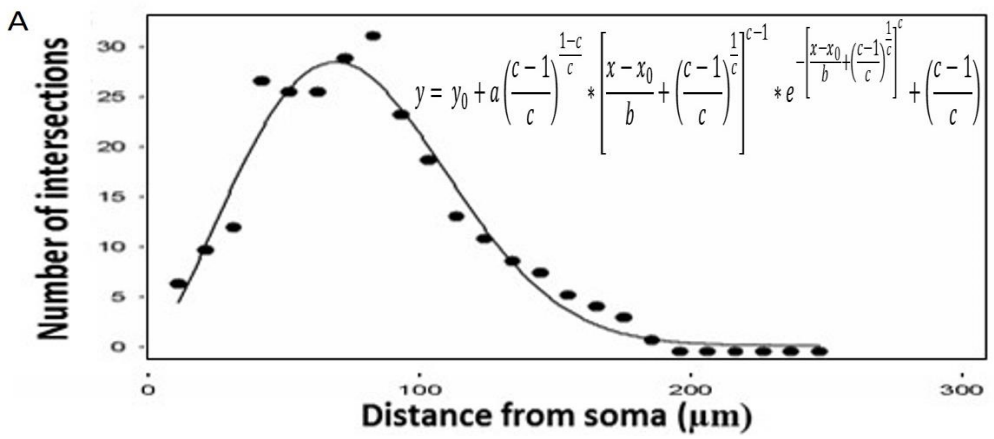
A
Number of intersections
Distance from soma (µm)
0
100
200
300
0
5
10
15
20
25
30

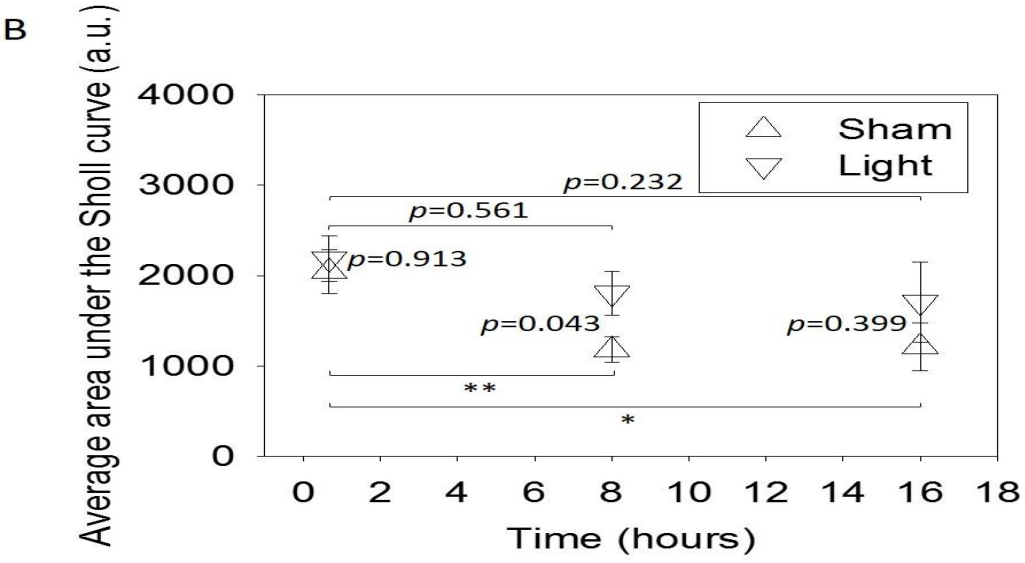
B
Average area under the Sholl curve (a.u.)
Time (hours)
Sham
Light
p=0.232
p=0.561
p=0.913
p=0.043
p=0.399
**
*
0
1000
2000
3000
4000
0
2
4
6
8
10
12
14
16
18

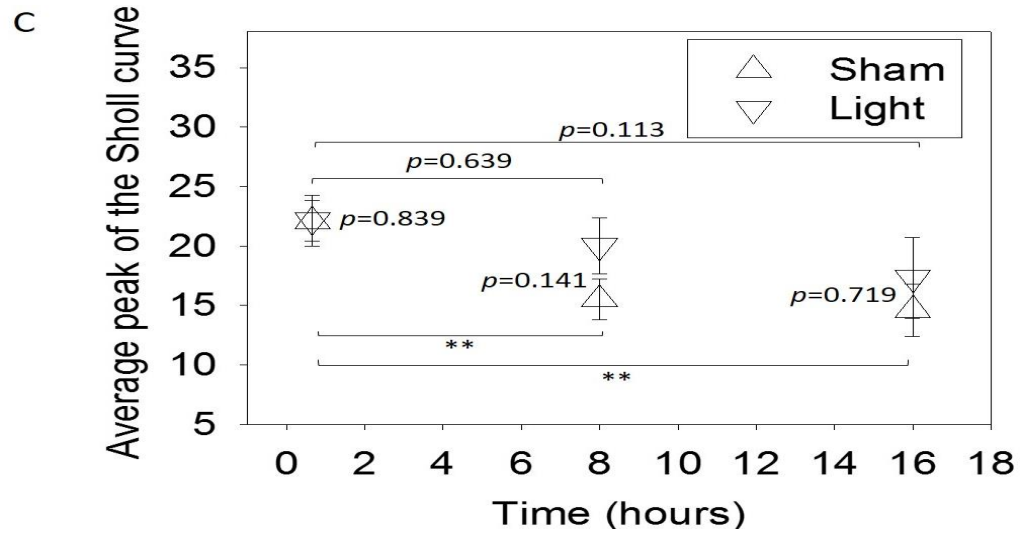
C
Average peak of the Sholl curve
Time (hours)
Sham
Light
p=0.113
p=0.639
p=0.839
p=0.141
p=0.719
**
**
5
10
15
20
25
30
35
0
2
4
6
8
10
12
14
16
18

Figure 3

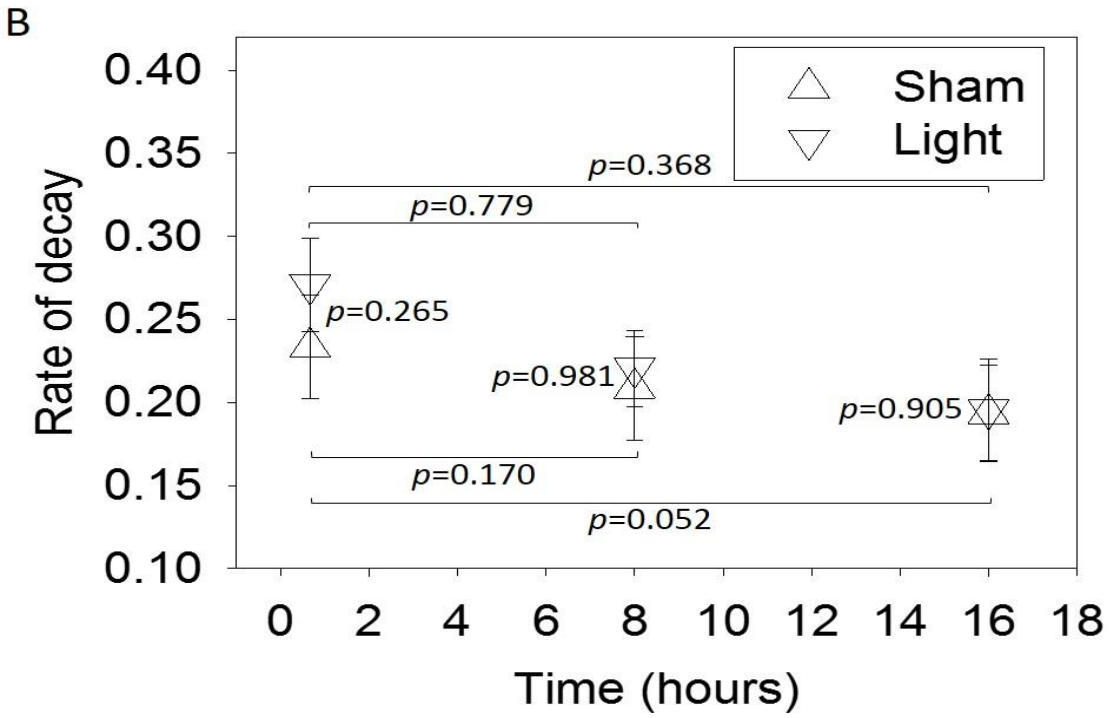
B
Rate of decay
0.40
0.35
0.30
0.25
0.20
0.15
0.10
Sham
Light
p=0.368
p=0.779
p=0.265
p=0.981
p=0.905
p=0.170
p=0.052
0
2
4
6
8
10
12
14
16
18
Time (hours)

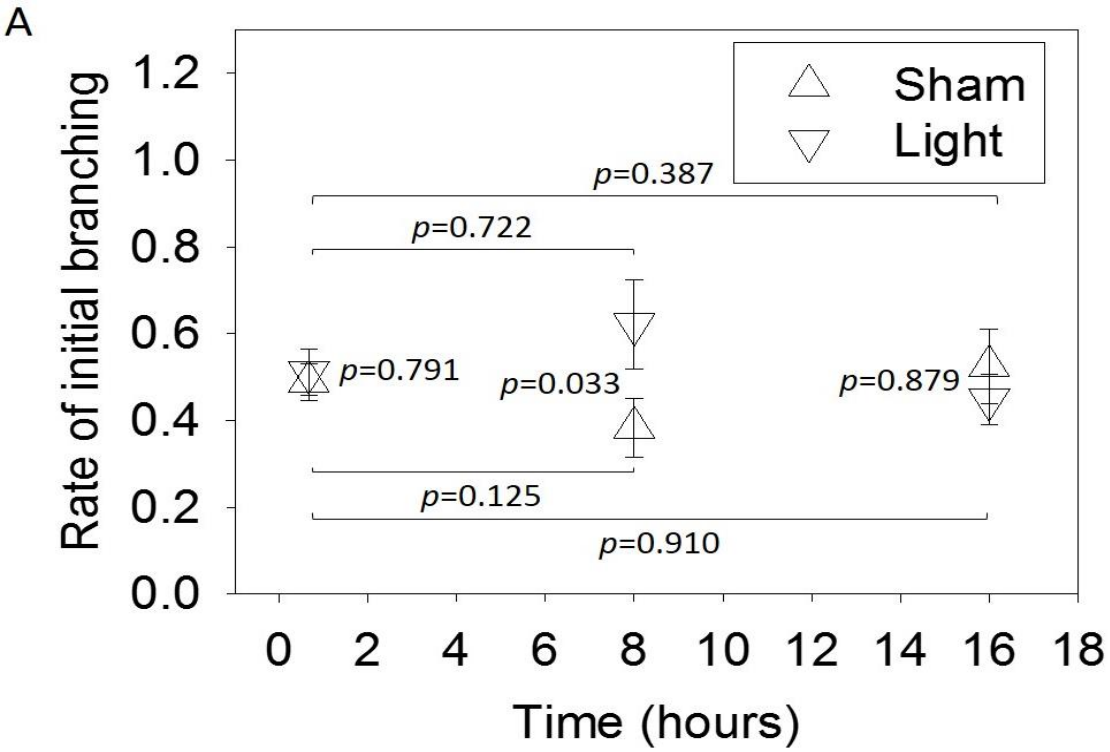
A
Rate of initial branching
1.2
1.0
0.8
0.6
0.4
0.2
0.0
Sham
Light
p=0.387
p=0.722
p=0.791
p=0.033
p=0.879
p=0.125
p=0.910
0
2
4
6
8
10
12
14
16
18
Time (hours)

Figure 4

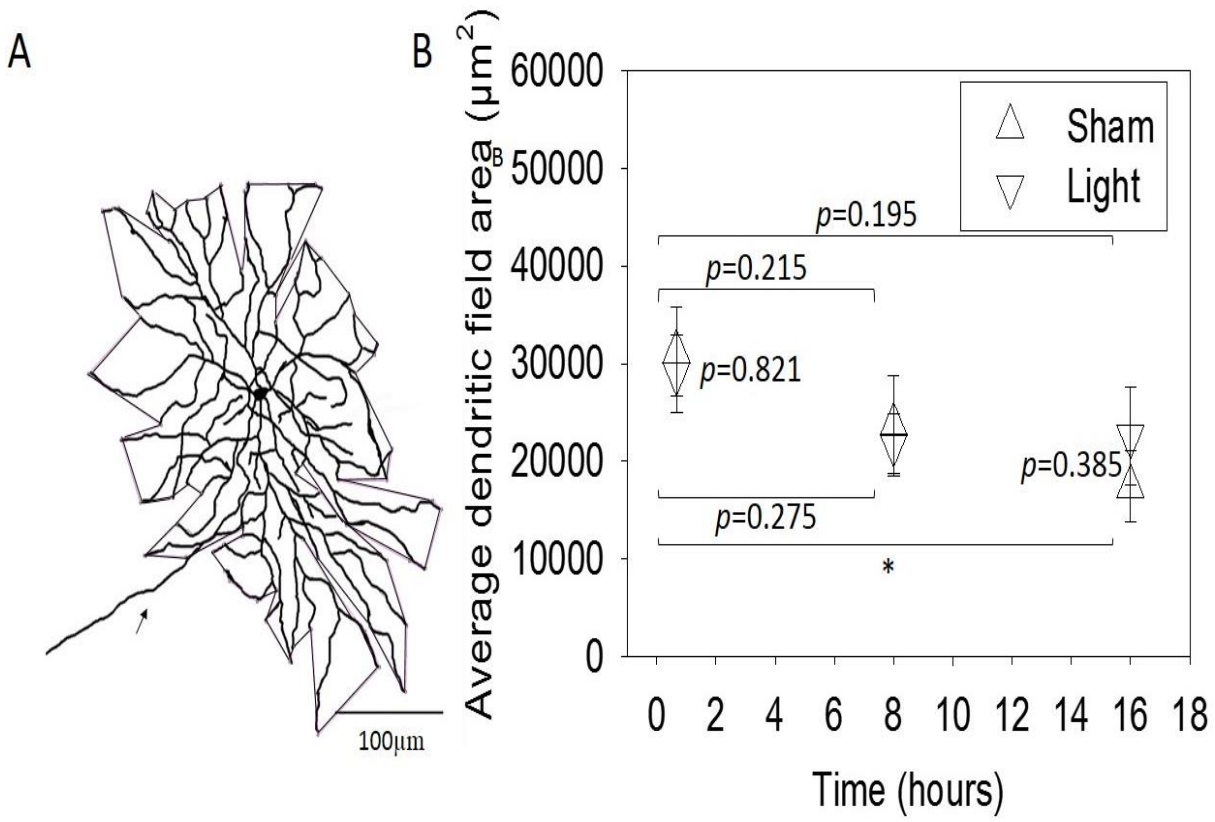
A
100µm
B
Average dendritic field area$_B$ (µm^2)
60000
50000
40000
30000
20000
10000
0
Sham
Light
p=0.195
p=0.215
p=0.821
p=0.385
p=0.275
*
0 2 4 6 8 10 12 14 16 18
Time (hours)

Figure 5

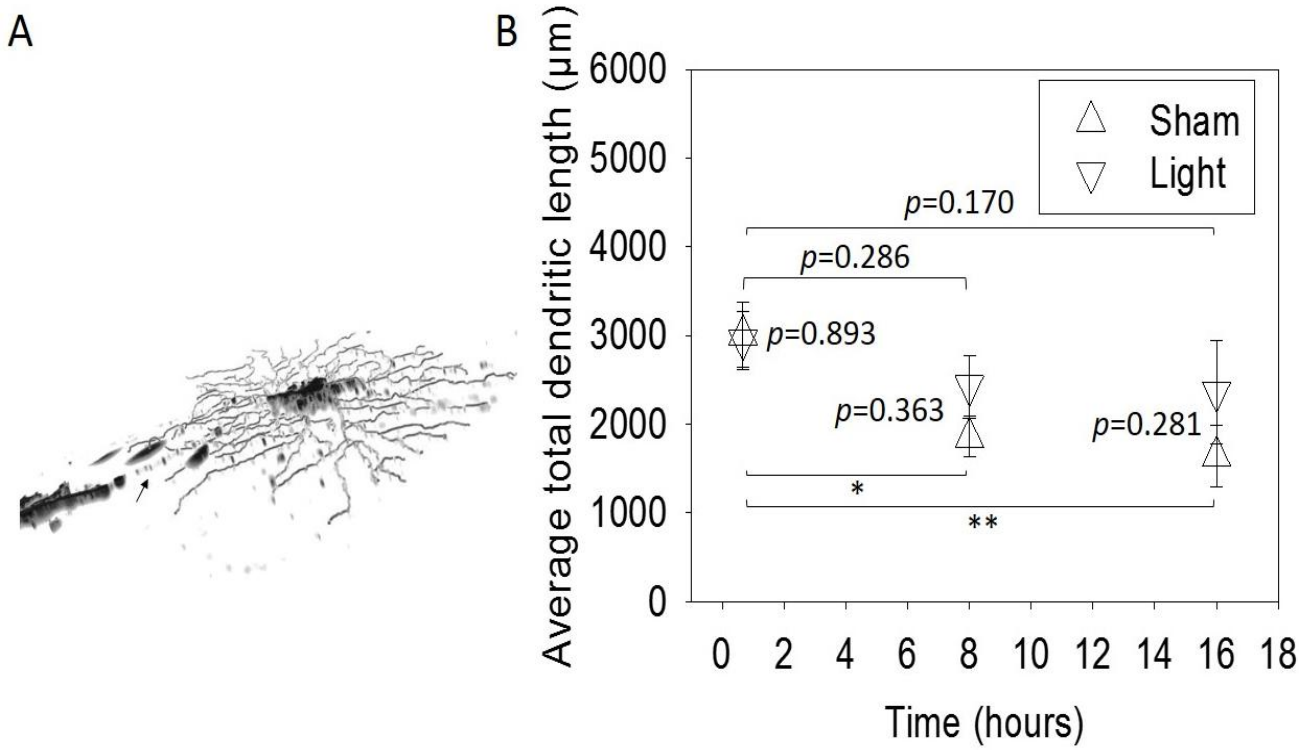
A
B
Average total dendritic length (µm)
6000
5000
4000
3000
2000
1000
0
Sham
Light
p=0.170
p=0.286
p=0.893
p=0.363
p=0.281
*
**
0
2
4
6
8
10
12
14
16
18
Time (hours)